Chemie der Erde 74 (2014) 705–713

Contents lists available at ScienceDirect

Chemie der Erde

journal homepage: www.elsevier.de/chemer

Lithium elemental and isotopic variations in rock-melt interaction

Ben-Xun Su[a,b,c,*], Hong-Fu Zhang[a], Etienne Deloule[b], Nathalie Vigier[b], Patrick Asamoah Sakyi[d]

[a] State Key Laboratory of Lithospheric Evolution, Institute of Geology and Geophysics, Chinese Academy of Sciences, Beijing 100029, China
[b] Centre National de la Recherche Scientifique, CRPG, BP20, 54501 Vandoeuvre-Les-Nancy Cedex, France
[c] Department of Earth Sciences, University of Hong Kong, Hong Kong, China
[d] Department of Earth Science, University of Ghana, P.O. Box LG 58, Legon, Accra, Ghana

ARTICLE INFO

Article history:
Received 25 September 2013
Accepted 20 April 2014
Editorial handling - A. Renno

Keywords:
Li isotopes
Xenocryst
Phenocrysts
Mantle metasomatism
Mineral–host magma interaction

ABSTRACT

Despite the occurrence of highly variable lithium (Li) elemental distribution and isotopic fractionation in mantle mineral, the mechanism of Li heterogeneity and fractionation remains a controversial issue. We measured Li contents and isotopic compositions of olivine and clinopyroxene xenocrysts and phenocrysts from kamafugite host lavas, as well as minerals in melt pockets occurring as metasomatic products in peridotite xenoliths from the Western Qinling, central China. The olivine xenocrysts in the kamafugites show compositional zonation. The cores have high Mg# ($100 \times Mg/(Mg+Fe)$; 91.0–92.2) and Li abundances (5.63–21.7 ppm), low CaO contents ($\leq$0.12 wt%) and low δ^7Li values (−39.6 to −6.76‰), which overlap with the compositional ranges of the olivines in the melt pockets as well as those in peridotite xenoliths. The rims of the olivine xenocrysts display relatively low Mg# (85.9–88.2), high CaO contents (0.19–0.38 wt%) and high δ^7Li values (18.3–26.9‰), which are comparable to the olivine phenocrysts (Mg#: 86.4–87.1; CaO: 0.20–0.28 wt%; Li: 12.4–36.8 ppm; δ^7Li: 18.1–26.0‰) and the silicate-melt metasomatized olivines. The clinopyroxene phenocrysts and clinopyroxenes in the melt pockets have no distinct characteristics with respect to the Li abundances and δ^7Li values, but show higher and lower CaO contents, respectively, than the clinopyroxenes from silicate and carbonatite metasomatized samples. These features indicate that Li concentration and isotopic signatures of the cores of the xenocrysts recorded carbonatite melt-peridotite reaction (carbonatite metasomatism) at mantle depth, and the variations in the rims probably resulted from xenocryst–host magma interaction during ascent. Our results reveal that the interaction with carbonatite and silicate melts gave rise to an increase in Li abundance in minerals of peridotite xenoliths at mantle depth or during transportation. In terms of δ^7Li, the carbonatite and silicate melts produced remarkably contrasting δ^7Li variations in olivine. Based on the systematic variations of Li abundances and Li isotopes in olivines, we suggest that the δ^7Li value of olivine is a more important indicator than that of clinopyroxene in discriminating carbonatite and silicate melt interaction agents with peridotites.

1. Introduction

The large mass difference between lithium (Li) isotopes, ^{6}Li and ^{7}Li, and its high diffusivity make it a powerful tracer of low-temperature weathering and water-rock interactions (Richter et al., 2003; Coogan et al., 2005; Teng et al., 2006; Vigier et al., 2009), whereas equilibrium Li isotope fractionation is expected at high temperatures (Tomascak et al., 1999; Magna et al., 2006; Jeffcoate et al., 2007), since no fractionation of Li isotopes was observed during basalt and granite differentiation at magma temperatures >1050 °C (Tomascak et al., 1999) and > 600 °C (Teng et al., 2006), respectively. Diffusion modeling results indicate that at mantle temperatures, 50 m-scale heterogeneities may disappear after few million years under certain conditions, however, at lower temperatures these heterogeneities may survive (Halama et al., 2007; Vlastélic et al., 2009). The range of δ^7Li in basalts, including mid-ocean ridge basalts, arc basalts and intra-plate basalts, and in peridotites is remarkably restricted (δ^7Li = 3–5‰), which suggests that the mantle may be fairly homogeneous in terms of its Li isotope composition (Chan et al., 1992, 2002; Chan and Frey, 2003; Elliott et al., 2006; Magna et al., 2006; Jeffcoate et al., 2007; Tomascak et al., 2008; Pogge von Strandmann et al., 2011).

* Corresponding author at: P.O. Box 9825, Beijing 100029, China.
Tel.: +86 10 82998514; fax: +86 10 62010846.
E-mail addresses: subenxun@mail.igcas.ac.cn, benxunsu@gmail.com (B.-X. Su).

http://dx.doi.org/10.1016/j.chemer.2014.04.005
0009-2819/

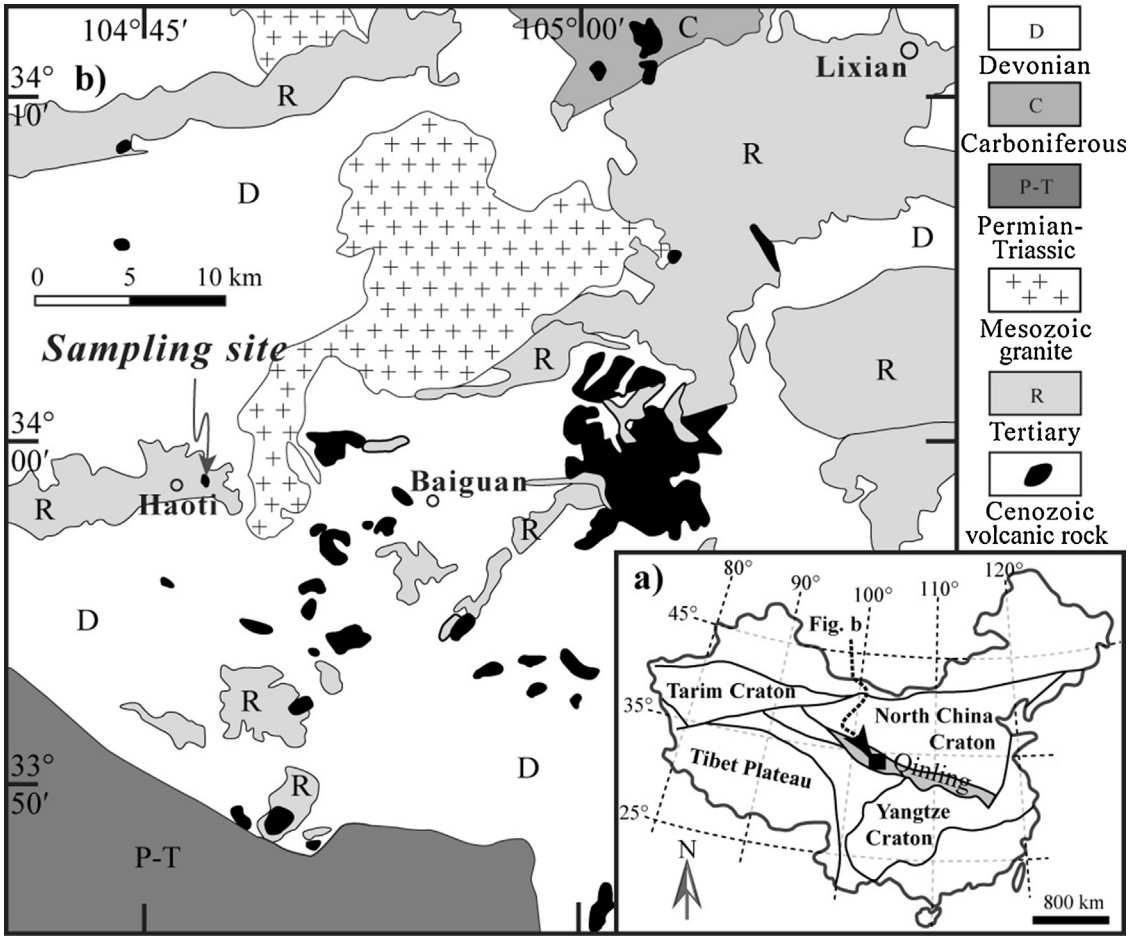

Fig. 1. (a) Generalized tectonic framework of China showing the major blocks and the location of the study area. (b) Geological map showing the distribution of Cenozoic kamafugites in the Western Qinling and sample locality.
Modified after Yu et al. (2004).

However, other studies have revealed extremely large Li isotopic variation within individual phenocrysts (Parkinson et al., 2007) and at intragranular, intergranular and intersample scales in mantle-derived rocks (Seitz et al., 2004; Nishio et al., 2004; Jeffcoate et al., 2007; Aulbach and Rudnick, 2009; Su et al., 2012a). Although large Li isotopic variation has been ascribed to mantle heterogeneity of Li isotopes and secondary processes such as melt/fluid metasomatism (Rudnick and Ionov, 2007; Wagner and Deloule, 2007; Vlastélic et al., 2009; Zhang et al., 2010; Tang et al., 2011; Krienitz et al., 2012; Su et al., 2012a; Ackerman et al., 2013), it has also been argued that the variation could also be caused by Li isotopic fractionation during cooling process (Coogan et al., 2005; Ionov and Seitz, 2008; Gallagher and Elliott, 2009; Caciagli et al., 2011) and xenolith/xenocryst–host magma interaction during ascent (Aulbach and Rudnick, 2009). There remain, however, a number of controversial issues and key among them has to do with which mechanism dominates the Li isotope variation recorded in the samples.

In this study, we present in situ Li isotopic data of zoned xenocrysts and phenocrysts in kamafugites as well as carbonatite metasomatic products in host peridotite xenoliths from the Western Qinling, central China. The results show large Li and δ^7Li variations in individual xenocrysts whose rims and cores are isotopically correlated to phenocrysts and metasomatic products, respectively. Thus, the primary composition could be preserved in the cores. This study also demonstrates distinct Li isotope fractionation trends of mantle materials that have experienced silicate and carbonatite metasomatism under mantle conditions and their interaction with host magmas during ascent.

2. Samples

The Western Qinling in central China is a unique locality where kamafugite and associated carbonatite outcrops occur as volcanic cones (Fig. 1; Yu et al., 2004; Su et al., 2009). These Cenozoic volcanic rocks (7–23 Ma) are distributed in the Tianshui-Lixian fault basin in the Western Qinling (Fig. 1B; Yu et al., 2004; Su et al., 2009, 2010a). Kamafugite is a potassic silica-undersaturated igneous rock consisting of matrix and phenocrysts including olivine, clinopyroxene, melilite, nephelite, phlogopite, calcite, apatite, etc. (Yu et al., 2004). Abundant xenocrysts and peridotite xenoliths are mainly entrained in the Haoti and Baiguan kamafugite cinder cones and have been studied extensively to decipher the nature and deep processes of the lithospheric mantle beneath the Western Qinling (Su et al., 2006, 2009, 2010a,b, 2011).

The xenocrysts and phenocrysts in the kamafugites from the Western Qinling can be recognized based on their distinct morphological and chemical features (Su et al., 2006). Olivine xenocrysts are commonly characterized by rounded and embayed crystal shape and well-developed cracks. Their sizes are mostly within the range of 200–900 μm and display apparent compositional zonations (Fig. 2a–c). The zoned texture was probably formed through rapid reaction with the host melt. The cores of the olivine xenocrysts have compositions (e.g., Mg# (100 × Mg/(Mg+Fe)) = 90–92) similar

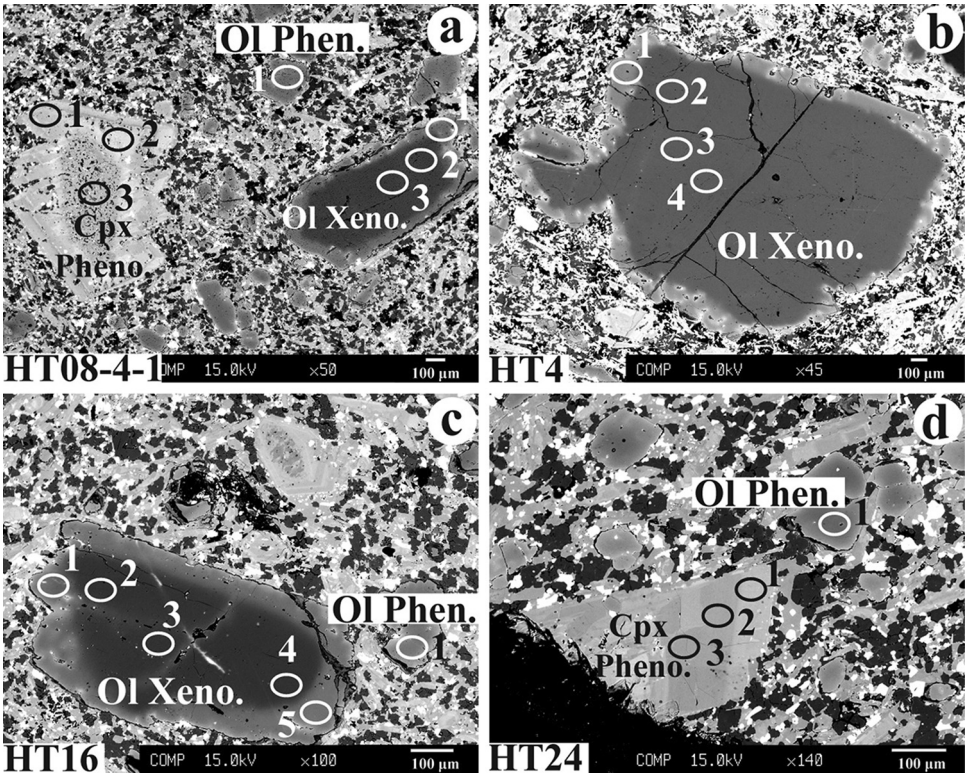

Fig. 2. Back-scattered images of olivine and clinopyroxene phenocrysts and xenocrysts in the Haoti kamafugites from the Western Qinling, central China, Ol Pheno, olivine phenocrysts; Ol Xeno, olivine xenocryst; Cpx Pheno, clinopyroxene phenocryst. The ellipse indicates the analyzed spot of electron microprobe and ion probe analyses, and the numbers represent the spot number corresponding to those in Table 1. See detailed description in the text.

to those of olivines from mantle peridotite xenoliths entrained in the kamafugites from the Western Qinling, whilst their rims (Mg# = 80–86) are compositionally identical to those of the olivine phenocrysts from the host kamafugites (Su et al., 2006). The textural characteristics as well as compositional features demonstrate that these olivine xenocrysts were disaggregated from the lithospheric peridotites (Zhang, 2005; Su et al., 2006). In contrast, the olivine phenocrysts are relatively fine-grained (<100 μm) and display well-defined boundaries with rare zoning texture (Fig. 2d). The clinopyroxene phenocrysts on the other hand, have variable sizes and rarely show zoning textures (Fig. 2a and d). These phenocrysts are rich in CaO, Al_2O_3 and trace elements, and depleted in Mg# (Su et al., 2006, 2011).

The Western Qinling peridotite xenoliths had been metasomatized by carbonatite melts before their entrainment, with melt pockets occurring as one of the metasomatic products (Fig. 3; Su et al., 2009, 2010a,b). The melt pockets are composed of secondary minerals such as olivine, clinopyroxene, feldspar, amphibole, calcite and ilmenite, and interpreted as the breakdown products of orthopyroxenes after interaction with melts (Fig. 3; Su et al., 2009, 2010b, 2012b). The mineral grains in the melt pockets are small in size (mostly less than 60 μm; Fig. 3) and have compositions distinct from those of the primary minerals in the peridotite xenoliths (Su et al., 2010b, 2012b).

3. Analytical methods

Major element compositions of minerals were determined by wavelength dispersive spectrometry using JEOL JXA8100 electron probe microanalyzer operating at an accelerating voltage of 15 kV and 10 nA beam current, 5 μm beam spot and 10–30 s counting time on peak. The precisions of all analyzed elements were better than 1.5%. Natural (jadeite [$NaAlSiO_6$] for Na, Al and Si, rhodonite [$MnSiO_3$] for Mn, sanidine [$KAlSi_3O_8$] for K, garnet [$Fe_3Al_2Si_3O_{12}$] for Fe, Cr-diopside [(Mg, Cr)$CaSi_2O_6$] for Ca, olivine [(Mg, Fe)$_2SiO_4$] for Mg) and synthetic (rutile for Ti, 99.7% Cr_2O_3 for Cr, Ni_2Si for Ni) minerals were used for standard calibration, and a program based on the ZAF procedure was used for matrix corrections.

Lithium contents and isotopic compositions were measured on gold-coated thin-sections using Cameca IMS-1270 ion microprobe in CRPG, Nancy, France. The primary beam was $^{16}O^-$ (15–30 nA, 30 μm diameter). Positive secondary ions with excess kinetic energies of 0 ± 20 eV were detected in pulse counting mode. A 180-s presputtering without raster was applied before analysis. The mass spectrometer was operated at a mass resolving power of 1500 ($M/\Delta M$). The primary beam position in the contrast aperture, the magnetic field and the energy offset were automatically centered before each measurement. Thirty cycles were measured with counting times of 12, 4 and 4 s for ^{6}Li, background at the 6.5 mass, and ^{7}Li, respectively. The counting rate for ^{7}Li ranged from 30,000 to 100,000 cps, depending on the Li content of the sample and the primary beam intensity. Olivine sample OlBZ29 and clinopyroxene sample CpxBZ226 (Decitre et al., 2002) were used as standards. The external 2σ errors of the isotope compositions for both the standards and the samples were less than 2‰. Li isotopes are given as δ^7Li (=$[(^7Li/^6Li)_{sample}/(^7Li/^6Li)_{L\text{-}SVEC} - 1] \times 1000$) relative to the standard NIST SRM 8545 (L-SVEC with $^7Li/^6Li = 12.0192$; Flesch et al., 1973; Decitre et al., 2002). The analyses of standard minerals in this study yielded homogeneous compositions and their δ^7Li values are −4.6 ± 0.7‰ (CpxBZ226),+4.4 ± 1.3‰ (OlBZ29) and −4.2 ± 0.5‰ (OpxBZ226), consistent with the previously reported values (Brooker et al., 2004; Zhang et al., 2010; Su et al., 2012a; Tang et al., 2012) and the recommended values of −4.1‰, +4.4‰ and −4.2‰, respectively (Decitre et al., 2002).

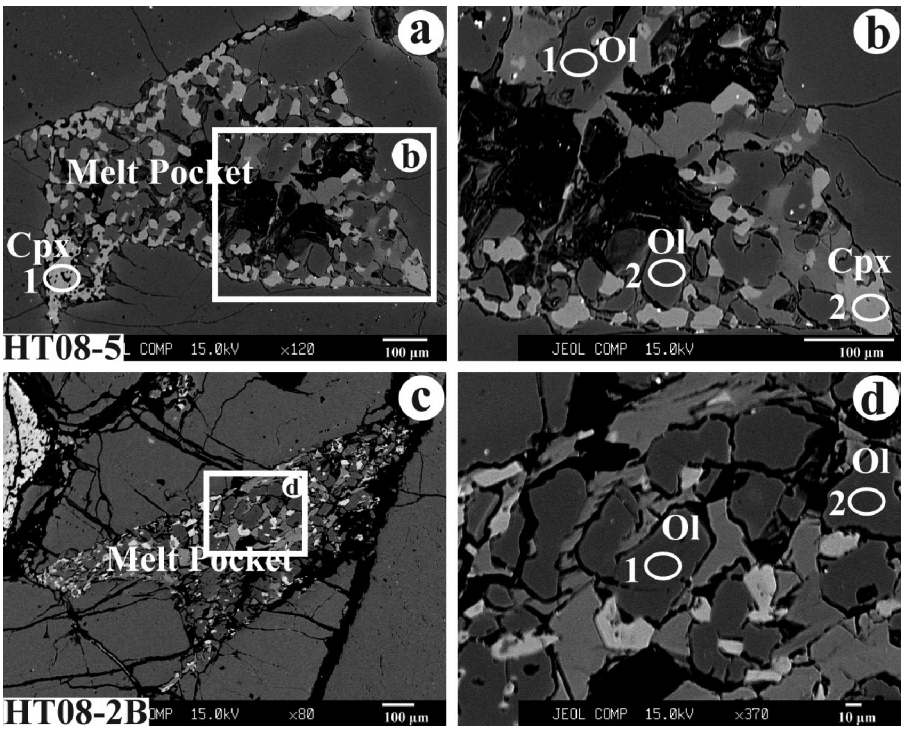

Fig. 3. Back-scattered images of olivine and clinopyroxene grains in the melt pockets of the carbonatite-metasomatized peridotite xenoliths entrained in the Haoti kamafugites from the Western Qinling, central China.

4. Results

4.1. Olivine

Three analyzed olivine xenocrysts in the kamafugites show compositional variations from core to rim. Their cores have high Mg# (91.0–92.2), low CaO contents (≤0.12 wt%) and low δ^7Li values (−39.6 to −6.76‰), whereas the rims display relatively low Mg# (85.9–88.2), high CaO contents (0.19–0.38 wt%) and high δ^7Li values (18.3–26.9‰) (Fig. 4 and Table 1). Lithium abundance varies considerably in core-to-rim profiles: decreasing from core (22 ppm) to rim (7 ppm) in two grains and increasing from core (6 ppm) to rim (39 ppm) in another grain (Fig. 4). Three olivine phenocrysts exhibit homogeneous compositions of Mg#: 86.4–87.1, CaO: 0.20–0.28 wt%, Li: 12.4–36.8 ppm, and δ^7Li: 18.1–26.0‰, which are similar to those of the rims of the olivine xenocrysts (Fig. 4 and Table 1). The olivines in the melt pockets have large variations in Li abundances (1.80–64.0 ppm) and δ^7Li values (−8.10 to 16.7‰), and relatively restricted Mg# (91.1–93.0) and CaO contents (0.07–0.15 wt%, except one grain having 1.41 wt%) (Table 1), all of which overlap with the compositional ranges of the cores of the olivine xenocrysts (Fig. 4).

4.2. Clinopyroxene

Two clinopyroxene phenocrysts show homogeneous compositions (Fig. 5). One grain has restricted ranges of Mg# (85.3–86.3), SiO_2 (50.3–50.7 wt%), Al_2O_3 (3.29–3.53 wt%), TiO_2 (1.87–1.89 wt%), CaO (23.5–23.9 wt%) and Na_2O (0.38–0.47 wt%) (Table 1). However, the other grain shows low Mg# (78.8–81.9) and SiO_2 (44.5–48.9 wt%), and high contents of Al_2O_3 (3.57–6.33 wt%), TiO_2 (2.50–4.34 wt%), and Na_2O (0.57–0.70 wt%). Two clinopyroxene

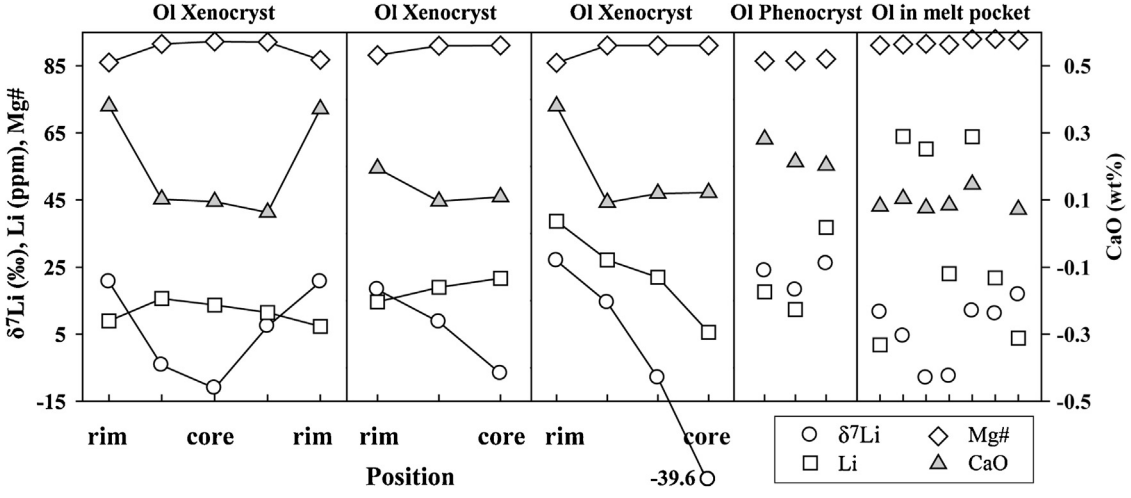

Fig. 4. Mg#, CaO, Li and δ^7Li compositions of olivine xenocrysts, phenocrysts and those in the melt pockets in the Haoti kamafugites from the Western Qinling, central China.

Table 1
Major (wt%) and Li elemental and Li isotopic compositions of olivine (Ol) and clinopyroxene (Cpx) xenocrysts and phenocrysts in the Haoti kamafugites from the Western Qinling.

Sample	Mineral	Position	Spot	δ^7Li/‰	2σ	Li/ppm	SiO_2	TiO_2	Al_2O_3	Cr_2O_3	FeO	MnO	MgO	CaO	Na_2O	K_2O	NiO	Total	Mg#
HT24	Ol phenocryst		1	23.9	1.7	17.7	40.3	0.06	0.04	0.04	13.0	0.22	46.1	0.28	0.06	0.00	0.26	100.4	86.4
HT16	Ol phenocryst		1	18.1	2.1	12.4	40.3	0.03	0.05	0.02	13.0	0.18	46.3	0.21	0.00	0.00	0.25	100.3	86.5
HT08-4-1	Ol phenocryst		1	26.0	2.0	36.8	39.5	0.04	0.05	0.06	12.4	0.14	46.5	0.20	0.00	0.00	0.25	99.2	87.1
HT16	Ol xenocryst	rim	1	20.6	1.8	8.96	39.6	0.01	0.02	0.04	13.3	0.13	45.5	0.38	0.04	0.00	0.25	99.2	86.0
			2	−4.27	1.8	15.6	40.8	0.04	0.01	0.03	8.34	0.11	50.0	0.10	0.00	0.00	0.33	99.8	91.5
		core	3	−11.1	1.9	13.7	41.1	0.04	0.01	0.06	7.74	0.16	50.9	0.10	0.04	0.00	0.34	100.5	92.2
			4	7.32	1.8	11.5	41.2	0.00	0.01	0.03	7.81	0.13	50.7	0.06	0.07	0.02	0.39	100.4	92.1
		rim	5	20.6	2.3	7.31	39.8	0.04	0.01	0.02	12.92	0.16	47.1	0.37	0.00	0.02	0.23	100.7	86.8
HT08-4-1	Ol xenocryst	rim	1	18.3	2.3	14.7	39.9	0.05	0.02	0.09	11.3	0.17	46.7	0.19	0.05	0.02	0.35	98.8	88.2
			2	8.66	2.3	19.0	40.2	0.04	0.02	0.03	8.76	0.09	49.0	0.10	0.03	0.00	0.40	98.7	91.0
		core	3	−6.76	2.1	21.7	40.8	0.00	0.01	0.01	8.84	0.12	50.0	0.11	0.01	0.03	0.36	100.3	91.0
HT4	Ol xenocryst	rim	1	26.9	1.7	38.7	40.6	0.00	0.03	0.01	13.5	0.24	45.7	0.38	0.01	0.03	0.31	100.8	85.9
			2	14.4	1.7	27.1	41.6	0.00	0.00	0.00	8.81	0.16	50.0	0.09	0.03	0.00	0.35	101.0	91.1
			3	−8.04	1.7	22.0	41.3	0.01	0.01	0.05	8.77	0.05	49.6	0.12	0.00	0.02	0.41	100.4	91.1
		core	4	−39.6	1.9	5.63	41.0	0.00	0.10	0.06	8.67	0.11	49.2	0.12	0.06	0.05	0.30	99.7	91.1
HT08-2B	Ol1 in melt pocket		1	11.5	2.1	1.80	40.8	0.00	0.00	0.10	8.71	0.18	49.6	0.08	0.01	0.03	0.18	99.7	91.1
	Ol2 in melt pocket		1	4.41	0.5	64.0	41.3	0.00	0.01	0.10	8.38	0.19	49.5	0.10	0.04	0.01	0.25	99.8	91.4
HT08-5	Ol1 in melt pocket		1	−8.10	0.9	60.2	41.0	0.01	0.01	0.13	8.23	0.15	49.6	0.08	0.07	0.02	0.19	99.5	91.6
	Ol2 in melt pocket		1	−7.59	1.1	23.0	41.1	0.02	0.01	0.12	8.41	0.15	49.1	0.08	0.05	0.00	0.16	99.1	91.3
HT16	Ol in melt pocket		1	11.9	1.8	63.9	41.6	0.09	0.00	0.04	7.01	0.17	51.4	0.15	0.00	0.04	0.23	100.7	93.0
HT08-4-1	Ol1 in melt pocket		1	11.1	2.7	21.8	43.0	0.00	0.24	0.74	6.30	0.14	46.6	1.41	0.67	0.16	0.10	99.4	93.0
	Ol2 in melt pocket		1	16.7	3.7	3.84	41.4	0.00	0.01	0.09	7.18	0.13	50.7	0.07	0.07	0.03	0.22	99.9	92.7
HT08-5	Cpx1 in melt pocket		1	8.55	1.6	4.22	54.3	0.42	0.18	4.11	2.02	0.09	16.7	18.3	2.04	0.00	0.06	98.2	93.7
	Cpx2 in melt pocket		1	7.78	2.5	3.31	54.9	0.13	0.15	4.56	1.89	0.14	16.1	19.0	2.19	0.04	0.00	99.1	93.9
HT24	Cpx phenocryst	rim	1	9.56	1.9	2.59	50.7	1.89	3.46	0.45	4.63	0.10	14.9	23.7	0.38	0.00	0.00	100.2	85.3
			2	11.9	1.6	6.99	50.6	1.89	3.29	0.47	4.28	0.03	15.0	23.9	0.44	0.00	0.05	99.9	86.3
		core	3	6.02	1.6	4.65	50.3	1.87	3.53	0.43	4.58	0.06	15.2	23.5	0.47	0.03	0.03	100.1	85.7
HT08-4-1	Cpx phenocryst	rim	1	9.60	3.0	1.08	45.1	3.86	6.33	0.12	6.24	0.03	12.9	23.6	0.67	0.02	0.01	98.8	78.8
			2	5.98	2.6	1.08	44.5	4.34	6.63	0.07	5.99	0.04	12.9	23.5	0.57	0.01	0.00	98.5	79.5
		core	3	4.80	2.8	1.37	48.9	2.50	3.57	0.00	5.55	0.10	13.9	23.7	0.70	0.03	0.00	99.1	81.9

Note: Mg# = 100 × Mg/(Mg+Fe).

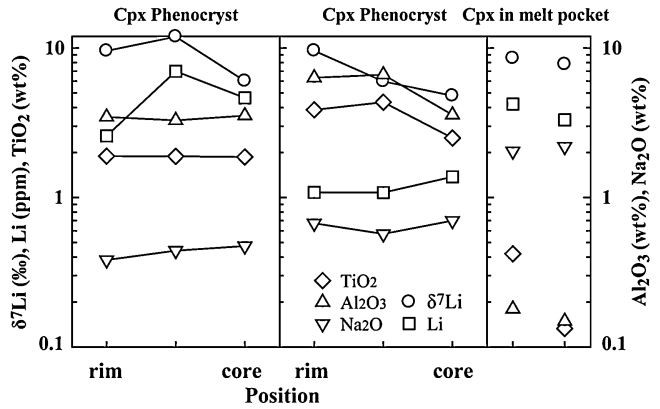

Fig. 5. Al_2O_3, TiO_2, Na_2O, Mg#, SiO_2, Li and δ^7Li compositions of clinopyroxene phenocrysts and those in the melt pockets in the Haoti kamafugites from the Western Qinling, central China.

grains in the melt pockets are compositionally different from the phenocrysts, particularly with respect to their high Mg# (93.7, 93.9), SiO_2 (54.3 wt%, 54.9 wt%), Cr_2O_3 (4.11 wt%, 4.56 wt%), and Na_2O (2.04 wt%, 2.19 wt%), and low Al_2O_3 (0.18 wt%, 0.15 wt%), TiO_2 (0.42 wt%, 0.13 wt%), and CaO (18.3 wt%, 19.0 wt%) (Fig. 5 and Table 1). Their enrichments in Na and Cr, high Mg# and depletions in Ti and Al are consistent with the metasomatic origin (Su et al., 2009, 2010a, b, 2011). However, Li concentrations (1.08–6.99 ppm) and Li isotopic compositions (4.80–11.9‰) of the clinopyroxenes do not correlate with their major element compositions (Table 1).

5. Discussion

5.1. Li and Li isotopic variations in cooling process and fractional crystallization

The diffusivity of Li isotopes, with ^{6}Li diffusing about 2–3% faster than ^{7}Li (Richter et al., 2003; Coogan et al., 2005; Lundstrom et al., 2005), is independent of physical factors and composition (i.e., temperature, pressure and melt composition). However, the diffusion rate of Li is highly variable in different minerals and may change with temperature (Wunder et al., 2006; Ionov and Seitz, 2008; Dohmen et al., 2010; Caciagli et al., 2011; Coogan, 2011; Yakob et al., 2012). Consequently, Li isotopic fractionation will be accompanied by the preferential incorporation of Li into minerals. A study by Ionov and Seitz (2008) showed that the anomalous and un-equilibrated Li isotopic compositions in peridotite xenoliths may be related to the re-distribution of Li between minerals, but the authors attributed it to the post-eruptional cooling process. They argued that most peridotite xenoliths and xenocrysts display uniform distributions of Li content (i.e., $Li_{olivine} < Li_{orthopyroxene} < Li_{clinopyroxene}$) and Li isotopic variations (i.e., $\delta^7Li_{olivine} > \delta^7Li_{orthopyroxene} > \delta^7Li_{clinopyroxene}$) between minerals because: (1) the rate of diffusion of Li in olivine is much slower than in pyroxene under the same conditions (Parkinson et al., 2007; Dohmen et al., 2010; Coogan, 2011; Yakob et al., 2012), and (2) Li partitioning changes with cooling as it diffuses from olivine into clinopyroxene with decreasing temperature (Ionov and Seitz, 2008). On the contrary, different trends in the variation of Li abundances and Li isotopic compositions in mantle peridotites, particularly the reverse sequence in carbonatite metasomatized samples, have been commonly observed (Woodland et al., 2004; Zhang et al., 2010; Su et al., 2012a, 2014; Tang et al., 2012).

The petrographic characteristics and chemical compositions (i.e., high CaO, low Mg#) of olivine and clinopyroxene in the Haoti kamafugites indicate their magmatic origin and phenocrystic nature (Fig. 2 and Table 1). Olivine phenocrysts show larger Li

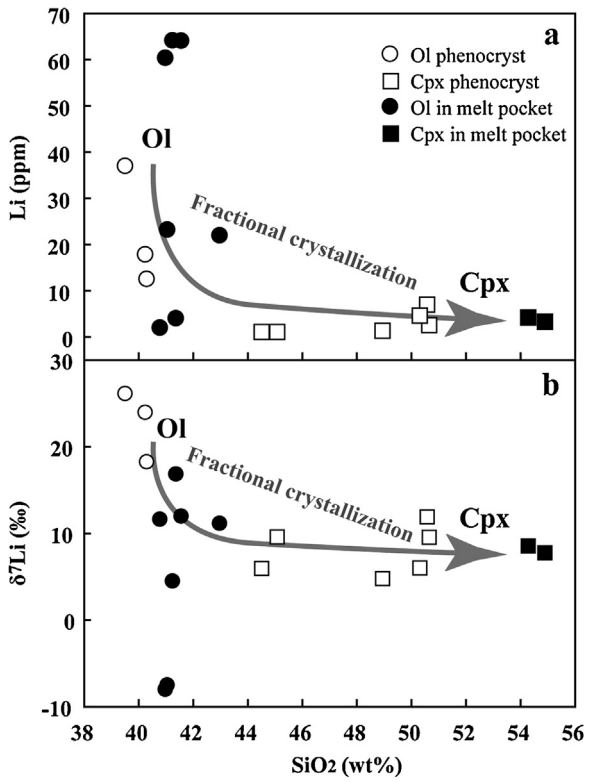

Fig. 6. SiO_2 versus Li (a) and SiO_2 versus δ^7Li (b) correlation diagrams for olivine and clinopyroxene phenocrysts and those in melt pockets. Fractional crystallization line is defined by general crystallization sequence of olivine first and then clinopyroxene in magmas/melts.

abundance and isotopic variations than clinopyroxene phenocrysts (Fig. 6). The olivine phenocrysts have consistently high Li abundances and δ^7Li values, whereas the clinopyroxene phenocrysts are relatively low in both Li content and δ^7Li with no significant zonation (Table 1 and Figs. 4–6). The olivine and clinopyroxene in the melt pockets in the peridotite xenoliths also show similar compositional features. Lithium abundance of the olivines in the melt pocket is apparently higher than that in clinopyroxenes (Fig. 6a), while these olivines have much larger δ^7Li ranges than the clinopyroxenes (Fig. 6b). Moreover, the core-to-rim profiles of Li and δ^7Li are significantly different among the phenocrysts, xenocrysts and olivines/pyroxenes in the peridotite xenoliths (Figs. 4 and 5 and Su et al., 2012a, 2014). These features are in contradiction to the cooling theory.

However, these compositional variations between olivine and clinopyroxene are probably relevant to fractional crystallization. It is known that olivine crystallizes prior to clinopyroxene in fractional crystallization of both melt pocket at mantle depth and magmas during ascent. The higher Li abundance in olivine than clinopyroxene (Fig. 6a) indicates that Li is incorporated into mineral in the early stage of melt/magma fractionation. This inference is consistent with the previous experimental and empirical results that Li is a moderate compatible element for olivine (Chan et al., 1992; Dohmen et al., 2010; Caciagli et al., 2011). The overall decreasing δ^7Li value from olivine to clinopyroxene implies that fractional crystallization can result in Li isotopic fractionation of the melts/magmas.

5.2. Li elemental variations in mantle metasomatism and xenocryst–host magma interaction

The low CaO contents (<0.10 wt%) of olivines in the Haoti and Hannuoba peridotite xenoliths which plot within the field defined

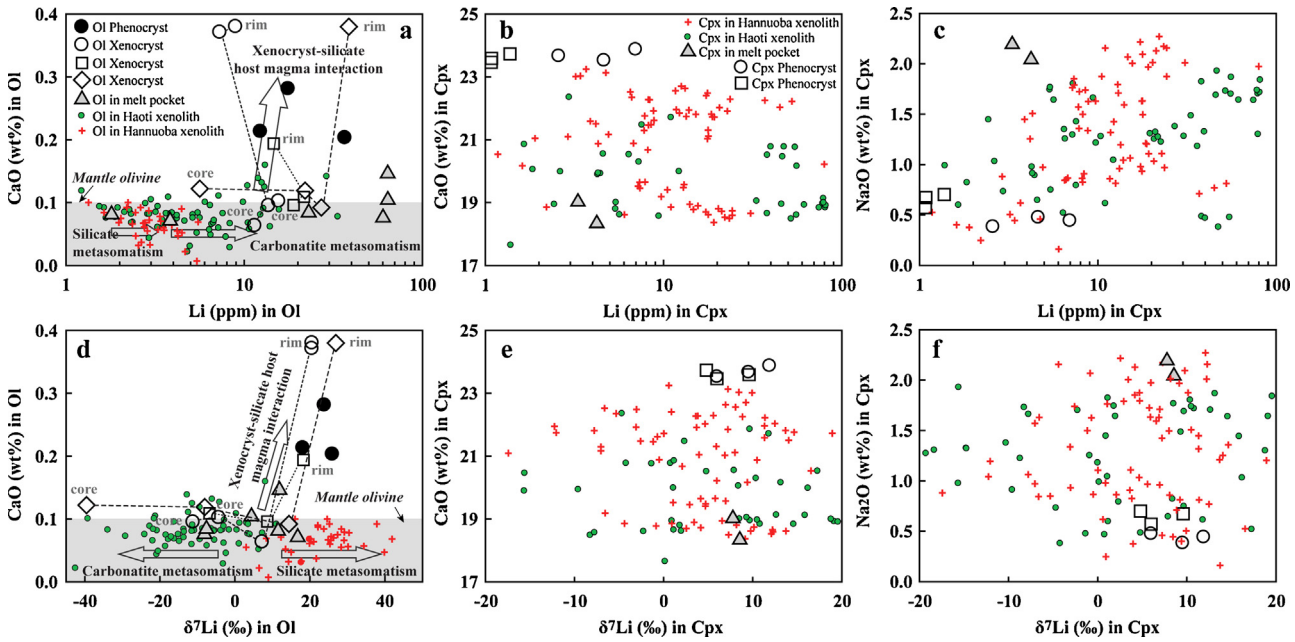

Fig. 7. Li and δ^7Li versus CaO and Na_2O correlation diagrams for olivines (a and d) and clinopyroxenes (b, c, e and f). Data for minerals in the Haoti (Western Qinling) and Hannuoba (North China Craton) xenoliths are from Su et al. (2012a), (2014). The samples from the Haoti and Hannuoba had been metasomatized by carbonatite and silicate melts, respectively. The gray field (CaO < 0.10 wt%) is defined for mantle olivines, whereas those olivines with CaO ≥ 0.10 wt% are of a magmatic origin (Thompson and Gibson, 2000). Both carbonatite and silicate metasomatic agents can increase the Li abundance, which is significant in the former, but does not change the CaO contents of the olivines. The interaction with host magmas during ascent increased the Li abundances as well as CaO of the olivines. Carbonatite metasomatism resulted in a decrease in the δ^7Li values of olivines, whereas silicate metasomatism and phenocryst-host silicate magma interaction increased the δ^7Li values remarkably. There is no significant difference among the effect of the three agents in the clinopyroxenes.

by the CaO contents of mantle olivines (Fig. 7a; Thompson and Gibson, 2000) suggest that Li enrichment and isotopic fractionation present in these samples occurred at mantle depth. Notably, the olivine xenocryst grain from sample HT4 displays different core-rim profiles for Li and δ^7Li, compared to the other two grains (Fig. 4), but exhibit identical Li compositions to the olivines in the peridotite xenoliths (Fig. 7a) probably due to its large grain size and lack of well-developed zonation (Fig. 2b). This olivine grain is ca. 1000 μm in diameter and did not experience considerable chemical exchange with the host magma during ascent. Considering the lower Li diffusion rate relative to Fe–Mg exchange in olivine (Parkinson et al., 2007), although the rim of the grain records the Fe–Mg reaction with the host magma, primitive Li signatures of carbonatite metasomatism at mantle depth are preserved in the whole grain (Fig. 7a). On the other hand, the Fe–Mg as well as Li composition of the other smaller grains is likely to be reset by the reaction with the host magma. In the following discussion, emphasis will be placed on the small-grained olivines with well-developed zonations to constrain the peridotite–host magma interaction.

Seitz and Woodland (2000) showed that olivines from equilibrated unmetasomatized peridotite xenoliths have Li abundances ranging between 1 and 2 ppm, while pyroxenes have Li contents from sub-ppm to 1.3 ppm. Metasomatized peridotites show highly variable Li content in both olivines and pyroxenes, such that Li distributions between olivine and clinopyroxene do not commonly achieve equilibrium (Seitz and Woodland, 2000; Aulbach and Rudnick, 2009; Zhang et al., 2010; Tang et al., 2011). The nature of the melt involved in mantle metasomatism plays a key role in preferential enrichment of Li in minerals (Seitz and Woodland, 2000; Seitz et al., 2004; Mallmann et al., 2009; Su et al., 2012a, 2014).

A general consensus is reached that mantle metasomatism causes an increase in Li abundances and isotopic re-distribution in mantle peridotites (Seitz and Woodland, 2000; Wagner and Deloule, 2007; Mallmann et al., 2009; Zhang et al., 2010; Tang et al., 2007, 2011, 2012; Su et al., 2012a). Compared to silicate metasomatism, carbonatite metasomatism can yield greater Li enrichment, particularly in olivine (Fig. 7a). Notably, the secondary olivine from the residual metasomatic melts in the melt pockets has up to 64 ppm Li that is extremely high compared with the coexisting clinopyroxene in the melt pocket and the primary olivine (Table 1 and Fig. 7a; Su et al., 2014). The Li abundances in the clinopyroxenes are variable in both metasomatic agents (Fig. 7b). The positive correlation between Na_2O and Li (Fig. 7c) suggests both silicate and carbonatite metasomatism could evaluate Li content of clinopyroxene as Na_2O is one of the important metasomatic parameters for peridotite (Su et al., 2010a). The distinct distribution of Li in minerals indicates that Li is preferentially incorporated into olivine relative to clinopyroxene during carbonatite metasomatism, which is different from silicate metasomatism, therefore corroborating the inferences made in previous studies (Seitz et al., 2004; Woodland et al., 2004; Jeffcoate et al., 2007; Tang et al., 2007; Zhang et al., 2010; Ackerman et al., 2013).

The cores of the olivine xenocrysts in the Haoti kamafugites show identical composition to the olivines in the peridotite xenoliths, indicating that these cores maintained the compositional signatures of carbonatite metasomatism at mantle depth, implying that cooling process did not significantly alter their mantle signatures. The presence of well-developed zoning texture, coupled with high-CaO and low-Mg# features indicate that the rims of the olivine xenocrysts recorded signatures of the interaction with the host magmas. The different core-to-rim profiles displayed in the three olivine xenocryst grains (Figs. 4 and 5) may imply that the variation trend in Li abundance and isotope compositions depends on the compositional differences between the xenocryst and the host magma. Thus, the xenocrysts preserve deep metasomatic signatures in the cores whilst their interaction with ascending host magmas is recorded in the rims.

5.3. Li isotopic variations in mantle metasomatism and xenocryst–host magma interaction

As discussed above, minerals experiencing the preferential incorporation of Li would have low δ^7Li values (Lundstrom et al., 2005; Wagner and Deloule, 2007; Teng et al., 2007; Wunder et al., 2007). This inference is clearly illustrated in Fig. 7d and e, in which the Haoti olivines metasomatized by carbonatite melt exhibit decreasing δ^7Li values with correspondingly high Li enrichment, whereas the Hannuoba olivines metasomatized by silicate melt are characterized by slight Li enrichment and high δ^7Li values (Fig. 7d). It has been established that metasomatic processes readily pump Li into mantle minerals from the melts, resulting in the depletion of ^{6}Li relative to ^{7}Li in the residual melts (Seitz and Woodland, 2000; Wagner and Deloule, 2007; Zhang et al., 2010; Tang et al., 2011). As a consequence, the olivines as well as clinopyroxenes in the melt pockets (representing residual melts) show generally high δ^7Li values (Table 1 and Fig. 7d and e). However, there is no distinction between Li isotopes in clinopyroxenes caused by carbonatite and silicate metasomatic agents (Fig. 7e and f). This may be interpreted by the modeling results of Aulbach and Rudnick (2009) which showed that δ^7Li of olivine can inherit the δ^7Li signature of the melt during peridotite–melt interaction, whilst clinopyroxene lags behind.

Similar to the Li abundance, the δ^7Li values in the cores of the olivine xenocrysts also overlap the compositional range of the olivines in the Haoti peridotite xenoliths, and the increasing trend of δ^7Li toward to the rims reflects the interaction between the xenocryst and the host magma (Fig. 7d), which is consistent with high δ^7Li values for host alkaline lavas containing mantle xenoliths reported by Magna et al. (2008) and Ackerman et al. (2013). Interestingly, the Li isotopic compositions in the rims of the olivine xenocrysts are very similar to those of the silicate-metasomatized olivines, although there are marked differences with respect to the CaO content and Li abundance (Fig. 7d). Considering the silicate nature of the host magmas, we suggest that the interaction with silicate melt would lead to an increase of δ^7Li in olivines, irrespective of mantle depth or ascending process, whereas the reverse trend would result from interaction between olivine and carbonatite melt. On the basis of the indistinguishable chemical compositions between clinopyroxenes and olivines that have experienced different levels of interactions, we suggest that compared to clinopyroxene, olivine records and preserves higher δ^7Li levels caused by different metasomatic agents.

6. Conclusions

The olivine xenocrysts entrained in the Haoti kamafugites from the Western Qinling exhibit systematic Li elemental and isotopic zonations. Their cores are characterized by significant Li enrichment and very low δ^7Li values, similar to the olivines in carbonatite-metasomatized peridotite xenoliths, while the rims are also rich in Li but with considerably high δ^7Li values which are comparable to the phenocrysts and those in the silicate-metasomatized peridotites. Integrating the zoning texture and major element chemistry, we infer that the Li elemental and isotopic signatures of the cores of the xenocrysts record carbonatite metasomatism at mantle depth, while the variations in the rims are attributed to xenocryst–host magma interaction during ascent. The distinct Li elemental and isotopic features in olivines compared to those in clinopyroxenes indicate that olivine is a better indicator than clinopyroxene in discriminating carbonatite and silicate metasomatic agents. We further conclude that the peridotite–melt interaction resulted in increased Li abundance that subsequently imparted variations to Li isotopes in the peridotite, whilst the carbonatite and silicate melts produced contrasting δ^7Li variations in olivine.

Acknowledgements

We are grateful to Qian Mao and Yuguang Ma for EPMA analyses and Raphaël Pik for the assistance in measurement of Li isotopes. The manuscript benefited from careful reviews by Tomas Magna as well as from editorial handling by Axel Renno and Alexander Deutsch. This work was financially supported by the National Natural Science Foundation of China (Grant Nos. 41173011, 91214203 and 41173009) and Hong Kong Scholars Program (No. XJ2012048).

References

Ackerman, L., SpaCek, P., Magna, T., Ulrych, J., Svojtka, M., Hegner, E., Balogh, K., 2013. Alkaline and carbonate-rich melt metasomatism and melting of subcontinental lithospheric mantle: Evidence from mantle xenoliths, NE Bavaria, Bohemian Massif. J. Petrol. 54, 2597–2633.

Aulbach, S., Rudnick, R.L., 2009. Origins of non-equilibrium lithium isotope fractionation in xenolithic peridotite minerals: examples from Tanzania. Chem. Geol. 258, 17–27.

Brooker, R.A., James, R.H., Blundy, J.D., 2004. Trace elements and Li isotope systematics in Zabargad peridotites: evidence of ancient subduction processes in the Red Sea mantle. Chem. Geol. 212, 179–204.

Caciagli, N., Brenan, J.M., McDonough, W.F., Phinney, D., 2011. Mineral-fluid partitioning of lithium and implications for slab-mantle interaction. Chem. Geol. 280, 384–398.

Chan, L.H., Edmond, J.M., Thompson, G., Gillis, K., 1992. Lithium isotopic composition of submarine basalts: implications for the lithium cycle in the oceans. Earth Planet. Sci. Lett. 108, 151–160.

Chan, L.H., Frey, F.A., 2003. Lithium isotope geochemistry of the Hawaiian plume: results from the Hawaiian scientific drilling project and Koolau Volcano. Geochem. Geophys. Geosyst. 4, http://dx.doi.org/10.1029/2002GC000365.

Chan, L.H., Leeman, W.P., You, C.F., 2002. Lithium isotopic composition of Central American volcanic arc lavas: implications for modification of subarc mantle by slab-derived fluids: correction. Chem. Geol. 182, 293–300.

Coogan, L.A., 2011. Preliminary experimental determination of the partitioning of lithium between plagioclase crystals of different anorthite contents. Lithos 125, 711–715.

Coogan, L.A., Kasemann, S.A., Chakraborty, S., 2005. Rates of hydrothermal cooling of new oceanic upper crust derived from lithium-geospeedometry. Earth Planet. Sci. Lett. 240, 415–424.

Decitre, S.E., Deloule, E., Reisberg, L., James, R., Agrinier, P., Mevel, C., 2002. Behavior of Li and its isotopes during serpentinization of oceanic peridotites. Geochem. Geophys. Geosyst. 3, http://dx.doi.org/10.1029/2001GC000178.

Dohmen, R., Kasemann, S.A., Coogan, L., Chakraborty, S., 2010. Diffusion of Li in olivine. Part I: Experimental observations and a multi species diffusion model. Geochim. Cosmochim. Acta 74, 274–292.

Elliott, T., Thomas, A., Jeffcoate, A., Niu, Y.L., 2006. Lithium isotope evidence for subduction-enriched mantle in the source of midocean-ridge basalts. Nature 443, 565–568.

Flesch, G.D., Anderson, A.R.J., Svec, H.J., 1973. A secondary isotopic standard for ^{6}Li/^{7}Li determinations. Int. J. Mass Spectrom. Ion Phys. 12, 265–272.

Gallagher, K., Elliott, T., 2009. Fractionation of lithium isotopes in magmatic systems as a natural consequence of cooling. Earth Planet. Sci. Lett. 278, 286–296.

Halama, R., McDonough, W.F., Rudnick, R.L., Keller, J., Klaudius, J., 2007. The Li isotopic composition of Oldoinyo Lengai: nature of the mantle sources and lack of isotopic fractionation during carbonatite petrogenesis. Earth Planet. Sci. Lett. 254, 77–89.

Ionov, D.A., Seitz, H.M., 2008. Lithium abundances and isotopic compositions in mantle xenoliths from subduction and intra-plate settings: mantle sources vs. eruption histories. Earth Planet. Sci. Lett. 266, 316–331.

Jeffcoate, A.B., Elliott, T., Kasemann, S.A., Ionov, D., Cooper, K., Brooker, R., 2007. Li isotope fractionation in peridotites and mafic melts. Geochim. Cosmochim. Acta 71, 202–218.

Krienitz, M.S., Garbe-Schonberg, C.D., Romer, R.L., Meixner, A., Haase, K.M., Stroncik, N.A., 2012. Lithium isotope variations in ocean island basalts: Implications for the development of mantle heterogeneity. J. Petrol. 53, 2333–2347.

Lundstrom, C.C., Chaussidon, M., Hsui, A.T., Kelemen, P., Zimmerman, M., 2005. Observations of Li isotopic variations in the Trinity ophiolite: evidence for isotopic fractionation by diffusion during mantle melting. Geochim. Cosmochim. Acta 69, 735–751.

Magna, T., Ionov, D.A., Oberli, F., Wiechert, U., 2008. Links between mantle metasomatism and lithium isotopes: Evidence from glass-bearing and cryptically metasomatized xenoliths from Mongolia. Earth Planet. Sci. Lett. 276, 214–222.

Magna, T., Wiechert, U., Halliday, A.N., 2006. New constraints on the lithium isotope compositions of the Moon and terrestrial planets. Earth Planet. Sci. Lett. 243, 336–353.

Mallmann, G., O'Neill, H.St., Klemme, C.S., 2009. Heterogeneous distribution of phosphorus in olivine from otherwise well-equilibrated spinel peridotite xenoliths

and its implications for the mantle geochemistry of lithium. Contrib. Mineral. Petrol. 158, 485–504.
Nishio, Y., Shunichi, N., Yamamoto, J., Sumino, H., Matsumoto, T., Prikhodko, V.S., Arai, S., 2004. Lithium isotopic systematics of the mantle-derived ultramafic xenoliths: implications for EM1 origin. Earth Planet. Sci. Lett. 217, 245–261.
Parkinson, I.J., Hammond, S.J., James, R.H., Rogers, N.W., 2007. High-temperature lithium isotope fractionation: Insights from lithium isotope diffusion in magmatic systems. Earth Planet. Sci. Lett. 257, 609–621.
Pogge von Strandmann, P.A.E., Elliott, T., Marschall, H.R., Coath, C., Lai, Y.J., Jeffcoate, A.B., Ionov, D.A., 2011. Variations of Li and Mg isotope ratios in bulk chondrites and mantle xenoliths. Geochim. Cosmochim. Acta 75, 5247–5268.
Richter, F.M., Davis, A.M., DePaolo, D.J., Watson, E.B., 2003. Isotope fractionation by chemical diffusion between molten basalt and rhyolite. Geochim. Cosmochim. Acta 67, 3905–3923.
Rudnick, R.L., Ionov, D.A., 2007. Lithium elemental and isotopic disequilibrium in minerals from peridotite xenoliths from fareast Russia: product of recent melt/fluid-rock reaction. Earth Planet. Sci. Lett. 256, 278–293.
Seitz, H.M., Brey, G.P., Lahaye, Y., Durali, S., Weyer, S., 2004. Lithium isotopic signatures of peridotite xenoliths and isotopic fractionation at high temperature between olivine and pyroxenes. Chem. Geol. 212, 163–177.
Seitz, H.M., Woodland, A.B., 2000. The distribution of lithium in peridotitic and pyroxenitic mantle lithologies—an indicator of magmatic and metasomatic processes. Chem. Geol. 166, 47–64.
Su, B.X., Zhang, H.F., Deloule, E., Sakyi, P.A., Xiao, Y., Tang, Y.J., Hu, Y., Ying, J.F., Liu, P.P., 2012a. Extremely high Li and low δ^7Li signatures in the lithospheric mantle. Chem. Geol. 292–293, 149–157.
Su, B.X., Zhang, H.F., Yang, Y.H., Sakyi, P.A., Ying, J.F., Tang, Y.J., 2012b. Breakdown of orthopyroxene contributing to melt pockets in mantle peridotite xenoliths from the Western Qinling, central China: constraints from in situ LA-ICP-MS mineral analyses. Mineral. Petrol. 104, 225–247.
Su, B.X., Zhang, H.F., Deloule, E., Vigier, N., Hu, Y., Tang, Y.J., Xiao, Y., Sakyi, P.A., 2014. Distinguishing silicate and carbonatite mantle metasomatism by using lithium and its isotopes (revision for publication).
Su, B.X., Zhang, H.F., Sakyi, P.A., Ying, J.F., Tang, Y.J., Yang, Y.H., Qin, K.Z., Xiao, Y., Zhao, X.M., 2010a. Compositionally stratified lithosphere and carbonatite metasomatism recorded in mantle xenoliths from the Western Qinling (Central China). Lithos 116, 111–128.
Su, B.X., Zhang, H.F., Sakyi, P.A., Qin, K.Z., Liu, P.P., Ying, J.F., Tang, Y.J., Malaviarachchi, S.P.K., Xiao, Y., Zhao, X.M., Mao, Q., Ma, Y.G., 2010b. Formation of melt pockets in mantle peridotite xenoliths from the Western Qinling (Central China): partial melting and metasomatism. J. Earth Sci. 21, 641–668.
Su, B.X., Zhang, H.F., Sakyi, P.A., Yang, Y.H., Ying, J.F., Tang, Y.J., Qin, K.Z., Xiao, Y., Zhao, X.M., Mao, Q., Ma, Y.G., 2011. The origin of spongy texture of mantle xenolith minerals from the Western Qinling, Central China. Contrib. Mineral. Petrol. 161, 465–482.
Su, B.X., Zhang, H.F., Xiao, Y., Zhao, X.M., 2006. Characteristics and geological significance of olivine xenocrysts in Cenozoic volcanic rocks from western Qinling. Prog. Nat. Sci. 16, 1300–1306.
Su, B.X., Zhang, H.F., Ying, J.F., Xiao, Y., Zhao, X.M., 2009. Nature and processes of the lithospheric mantle beneath the western Qinling: evidence from deformed peridotitic xenoliths in Cenozoic kamafugite from Haoti, Gansu Province, China. J. Asian Earth Sci. 34, 258–274.
Tang, Y.J., Zhang, H.F., Deloule, E., Su, B.X., Ying, J.F., Xiao, Y., Hu, Y., 2012. Slab-derived lithium isotopic signatures in mantle xenoliths from northeastern North China Craton. Lithos 149, 79–90.
Tang, Y.J., Zhang, H.F., Nakamura, E., Moriguti, T., Kobayashi, K., Ying, J.F., 2007. Lithium isotopic systematics of peridotite xenoliths from Hannuoba, North China Craton: implications for melt/rock interaction in the considerably thinned lithospheric mantle. Geochim. Cosmochim. Acta 71, 4327–4341.
Tang, Y.J., Zhang, H.F., Nakamura, E., Ying, J.F., 2011. Multistage melt/fluid-peridotite interactions in the refertilized lithospheric mantle beneath the North China Craton: constraints from the Li–Sr–Nd isotopic disequilibrium between minerals of peridotite xenoliths. Contrib. Mineral. Petrol. 161, 845–861.
Teng, F.Z., McDonough, W.F., Rudnick, R.L., Walker, R.J., 2006. Diffusion-driven extreme lithium isotopic fractionation in country rocks of the Tin Mountain pegmatite. Earth Planet. Sci. Lett. 243, 701–710.
Teng, F.Z., McDonough, W.F., Rudnick, R.L., Wing, B.A., 2007. Limited lithium isotopic fractionation during progressive metamorphic dehydration in metapelites: a case study from the Onawa contact aureole. Maine. Chem. Geol. 239, 1–12.
Thompson, R.N., Gibson, S.A., 2000. Transient high temperatures in mantle plume heads inferred from magnesian olivines in Phanerozoic picrites. Nature 407, 502–506.
Tomascak, P.B., Langmuir, C.H., le Roux, P., Shirey, S.B., 2008. Lithium isotopes in global mid-ocean ridge basalts. Geochim. Cosmochim. Acta 72, 1626–1637.
Tomascak, P.B., Tera, F., Helz, R.T., Walker, R.J., 1999. The absence of lithium isotope fractionation during basalt differentiation: new measurements by multi-collector sector ICP-MS. Geochim. Cosmochim. Acta 63, 907–910.
Vigier, N., Gislason, S.R., Burton, K.W., Millot, R., Mokadem, F., 2009. The relationship between riverine lithium isotope composition and silicate weathering rates in Iceland. Earth Planet. Sci. Lett. 287, 434–441.
Vlastélic, I., Koga, K., Chauvel, C., Jacques, G., Télouk, P., 2009. Survival of lithium isotopic heterogeneities in the mantle supported by HIMU-lavas from Rurutu Island, Austral Chain. Earth Planet. Sci. Lett. 286, 456–466.
Wagner, C., Deloule, E., 2007. Behaviour of Li and its isotopes during metasomatism of French Massif Central lherzolites. Geochim. Cosmochim. Acta 71, 4279–4296.
Woodland, A.B., Seitz, H.M., Yaxley, G.M., 2004. Varying behaviour of Li in metasomatised spinel peridotite xenoliths from western Victoria, Australia. Lithos 75, 55–66.
Wunder, B., Meixner, A., Romer, R.L., Feenstra, A., Schettler, G., Heinrich, W., 2007. Lithium isotope fractionation between Li-bearing staurolite, Li-mica and aqueous fluids: an experimental study. Chem. Geol. 238, 277–290.
Wunder, B., Meixner, A., Romer, R.L., Heinrich, W., 2006. Temperature-dependent isotopic fractionation of lithium between clinopyroxene and high pressure hydrous fluids. Contrib. Mineral. Petrol. 151, 112–120.
Yakob, J.L., Feineman, M.D., Deane Jr., J.A., Eggler, D.H., Penniston-Dorland, S.C., 2012. Lithium partitioning between olivine and diopside at upper mantle conditions: an experimental study. Earth Planet. Sci. Lett. 329–330, 11–21.
Yu, X.H., Zhao, Z.D., Mo, X.X., Wang, Y.L., Xiao, Z., Zhu, D.Q., 2004. Trace element, REE and Sr, Nd, Pb isotopic geochemistry of Cenozoic kamafugites and carbonatite from west Qinling, Gansu Province: implication of plume-lithosphere interaction. Acta Petrol. Sin. 20, 483–494 (in Chinese with English abstract).
Zhang, H.F., 2005. Transformation of lithospheric mantle through peridotite–melt reaction: a case of Sino-Korean craton. Earth Planet. Sci. Lett. 237, 768–780.
Zhang, H.F., Deloule, E., Tang, Y.J., Ying, J.F., 2010. Melt/rock interaction in remains of refertilized Archean lithospheric mantle in Jiaodong Peninsula, North China Craton: Li isotopic evidence. Contrib. Mineral. Petrol. 160, 261–277.